ЯДЕРНА ФІЗИКА
NUCLEAR PHYSICS

УДК 539.142 https://doi.org/10.15407/jnpae2020.01.038

Ali A. Abdul Hasan[1], Ehsan M. Raheem[1,*], Saad S. Dawood[1], Aqeel M. Jary[1], Rasha Z. Ahmed[2]

[1] Ministry of Science and Technology, Directorate of Nuclear Researches and Applications, Baghdad, Iraq
[2] University of Baghdad, College of Education for Women, Department of Human Resources, Baghdad, Iraq

*Corresponding author: ehsan.nucl@yahoo.com

NUCLEAR STRUCTURE STUDY OF EVEN-EVEN $^{24-42}$Si ISOTOPES USING SKYRME - HARTREE - FOCK AND HARTREE - FOCK - BOGOLYUBOV METHODS

The nuclear ground-state properties and the nuclear deformation of some even-even Silicon isotopes have been investigated. The spherical Skyrme - Hartree - Fock method that includes Hartree - Fock calculations in addition to several common Skyrme parameterizations, such as SkB, SkM*, SkE, SkX, SLy4, Skxta, SkP, UNEDF0, and UNEDF1, has been used to calculate the nuclear ground-state charge density distributions and the associated charge radii for ^{28}Si and ^{30}Si, because of the availability of the experimental data for these two stable isotopes. Furthermore, the mass, neutron and proton densities with the associated radii, the binding energies, the neutron skin thickness, and the charge form factors have been calculated for $^{24-42}$Si isotopes using SkM* parameterization. The quadrupole deformations of the selected isotopes have been investigated in terms of the potential energy curves that were deduced as a function of the quadrupole deformation parameters using the axially deformed configurational Hartree - Fock - Bogolyubov calculations with SkM* parameterization.

Keywords: nuclear ground-state properties, Skyrme - Hartree - Fock, Hartree - Fock - Bogolyubov, quadrupole deformation, silicon isotopes.

1. Introduction

The theoretical nuclear physics is aimed to study and understand the nuclear structure of systems that consist of individual interacted nucleons. Nuclear models are suggested to compile collective and detailed concepts of nuclear structure and to study the static and dynamic nuclear properties of nuclei. The self-consistent mean-field models with appropriate effective interactions are proposed to describe the movement of nucleons in an average potential and consequently to describe the nuclear ground-state properties and low-energy dynamics, where these models are derived in terms of the nucleon-nucleon interaction [1, 2]. One of the most popular interactions is the phenomenological Skyrme effective interaction [3] which is associated with Hartree - Fock (HF) calculations to make it feasible in nuclear physics and to provide a precise description of the nuclear ground-state properties [4, 5]. The self-consistent Skyrme - Hartree - Fock model (SHF) has been considered as a model that applied successfully in explaining the nuclear deformations of the stable nuclei near the valley of stability. The SHF calculations have the important advantage of reproducing the binding energies, nuclear densities and the corresponding radii, where electron scattering experiments investigated these quantities extensively [6]. With high-energy electron scattering experiments, the scattering cross-sections can directly be related to the charge, current and magnetization densities and thus related to the nuclear structures of these nuclei. The nuclear charge density distributions (CDD) and the related form factors provide a comprehensive perception of the spatial distribution of the nuclear charge, where these quantities have the same amount of data [7].

Pairing effects are considered for the unstable nuclei or these located near the driplines. These effects are incorporated within the Hartree - Fock - Bogolyubov (HFB) theory [8]. The HFB is considered as an extended version of the standard HF and provides a generalized single-particle theory that can be used to describe aspects of deformations in addition to pairing correlations due to the short-ranged attraction, while the HF plus the conventional Bardeen - Cooper - Schrieffer (BCS) approximation [9] is not suitable for the weakly bound systems. The BCS method fails in treating the pairing correlations in unstable nuclei because of the leakage of nucleons into the continuum states. To describe deformation, the HFB equation can be solved for deformed nuclei by expanding the quasiparticle wave functions using the axially transformed harmonic oscillator (THO) bases states [10, 11]. The solution is carried out using the HFBTHO code [12], where the Hamiltonian of the HFB that depends on the selected Skyrme interactions and paring effects is diagonalized to deduce the self-consistent solution.

The nuclear structure of some isotopes has been investigated by some recent researches using the SHF method. The nuclear binding energy and density

distributions of Pb isotopes have been studied by Yulianto et al. [13]. Radii and density calculations of ^{209}Bi nucleus have been performed by Yulianto et al. [14]. Abdullah [15] studied the matter density distributions and elastic electron scattering form factors of ^{6}He, ^{11}Li, ^{12}Be and ^{14}Be two-neutron halo nuclei using SHF method with MSk7 Skyrme force. Taqi et al. [16] investigated the ground and transition properties of ^{40}Ca and ^{48}Ca nuclei. Alzubadi et al. [17] used the SHF method to study the nuclear structure of ^{17}O nucleus. HFB method has been used recently to study the nuclear structure of some nuclei. Bayram et al. [18] calculated the values of total binding energies and quadrupole deformation parameters for even-even $^{112-134}$Te isotopes using HFB with Sly4 force. El Bassem et al. [19] employed the HFB method with Sly5 Skyrme force to study the ground-state properties of even-even and odd Nd, Ce and Sm isotopes. El Bassem et al. [20] applied the HFB method with Sly4 force to study the ground-state properties of even-even and odd Mo and Ru isotopes. Ouhachi et al. [21] studied the nuclear structure of neutron-rich Mn isotopes using HFB method with SLy4, SLy5, and SLy5T Skyrme effective interactions.

In the present work, the charge, mass, neutron and proton densities with the corresponding root mean square (rms) radii, the charge form factors, the binding energies, and the neutron skin thickness have been calculated for even-even $^{24-42}$Si nuclei using SHF method with the aid of several Skyrme parameterizations. The quadrupole deformations of the considered isotopes have been investigated using the HFB method with SkM* parameterization.

2. Theory

Many nuclear properties were studied extensively in recent years using the HF calculations in addition to the widespread applied Skyrme effective forces that succeeded in studying these properties in a wide range of the nuclear chart. The Skyrme force consists of two parts; the first part $v_{ij}^{(2)}$ is the momentum dependent two-body part, and the second part $v_{ijk}^{(3)}$ is the zero-range three-body part. The SHF Hamiltonian is defined as [4, 22]:

$$\hat{H} = \sum_i \hat{t}_i + \sum_{i<j} \hat{\upsilon}_{ij}^{(2)} + \sum_{i<j<k} \hat{\upsilon}_{ijk}^{(3)}, \qquad (1)$$

with

$$\hat{t}_i = \frac{\hat{P}_i^2}{2m}, \qquad (2)$$

$$\upsilon_{ij}^{(2)} = t_0\left(1 + x_0 \hat{\mathrm{P}}_\sigma\right)\delta_{\mathrm{ij}} + \frac{1}{2}t_1\left[\delta_{\mathrm{ij}}\hat{\vec{k}}^2 + \hat{\vec{k}}'^2\delta_{\mathrm{ij}}\right] +$$

$$+\ t_2\hat{\vec{k}}'^2\delta_{\mathrm{ij}}\hat{\vec{k}} + it_4\left(\hat{\vec{\sigma}}_i + \hat{\vec{\sigma}}_j\right)\cdot\hat{\vec{k}}'\delta_{\mathrm{ij}}\hat{\vec{k}}, \qquad (3)$$

$$\upsilon_{ijk}^{(3)} = t_3\,\delta_{ij}\,\delta_{jk}, \qquad (4)$$

where $\delta_{\mathrm{ij}} = \left(r_i - r_j\right)$, $\delta_{jk} = \left(r_j - r_k\right)$ are the Dirac delta functions and $\hat{\vec{\sigma}}$ are the Pauli spin matrices. The spin-exchange operator $\hat{P}_\sigma$ is given by

$$\hat{P}_\sigma = \frac{1}{2}\left(1 + \hat{\vec{\sigma}}_i\cdot\hat{\vec{\sigma}}_j\right). \qquad (5)$$

For even-even spin saturated nuclei, we have

$$\upsilon_{ijk}^{(3)} \approx \upsilon_{ij}^{(2)} = \frac{1}{6}t_3\left(1 + \hat{P}_\sigma\right)\rho_0^\alpha\left(R\right)\delta_{ij}, \qquad (6)$$

where $\rho_0\left(R\right)$ is the isoscalar density. The vectors $\hat{\vec{k}}$ and $\hat{\vec{k}}'$ are the relative (momentum) wave vector operators of two nucleons acting to the right and the left, respectively, and given by

$$\hat{\vec{k}} = \frac{1}{2i}\left(\vec{\nabla}_i - \vec{\nabla}_j\right), \quad \hat{\vec{k}}' = -\frac{1}{2i}\left(\vec{\nabla}_i - \vec{\nabla}_j\right). \qquad (7)$$

The density-dependent Skyrme interaction has the form [23]

$$\hat{V}_{Skyrme}\left(R,r\right) = t_0\left(1 + x_0\hat{P}_\sigma\right)\delta\left(r\right) +$$

$$+\frac{1}{6}t_3\left(1 + x_3\hat{P}_\sigma\right)\rho_0^\alpha\left(R\right)\delta\left(r\right) +$$

$$+\frac{1}{2}t_1\left(1 + x_1\hat{P}\sigma\right)\left[\hat{k}'^2\,\delta\left(r\right) + \delta\left(r\right)\hat{k}^2\right] +$$

$$+t_2\left(1 + x_2\hat{P}_\sigma\right)\hat{k}'\cdot\delta\left(r\right)\hat{k} + iW_0\left(\hat{\sigma}_i + \hat{\sigma}_j\right)\cdot\hat{k}'\cdot\delta\left(r\right)\hat{k}, \qquad (8)$$

where $R = \left(r_i - r_j\right)/2$ and $r = r_i - r_j$ are the center of mass coordinates and the relative distance, respectively. t_0, t_1, t_2, t_3, W_0, x_0, x_1, x_2, x_3 and α are the Skyrme free parameters describing the strengths of different interaction terms. These parameters are determined from the comparison between the calculated and the experimental nuclear ground-state properties such as binding energies, nucleon densities and root mean square radii.

In the SHF method, the total binding energy is expressed by the sum of kinetic, Skyrme, Coulomb, pairing energies in addition to the correction of the spurious motion [24].

$$E = \varepsilon_{kin} + \varepsilon_{Sky} + \varepsilon_{Coul} + \varepsilon_{Pair} - \varepsilon_{cm}. \qquad (9)$$

The kinetic energy of the nucleons is given by [25]:

$$\varepsilon_{kin} = \int d^3r \left(\frac{\hbar^2}{2m_p}\tau_p + \frac{\hbar^2}{2m_n}\tau_n \right), \qquad (10)$$

where τ_n and τ_p are the kinetic energy densities of neutrons and protons, respectively.

The Skyrme energy takes the form [26]

$$\varepsilon_{Sky} = \int d^3r \left\{ \frac{\hbar^2}{2m}\tau + \frac{1}{2}t_0\left[\left(1+\frac{1}{2}x_0\right)\rho^2 - \left(x_0+\frac{1}{2}\right)\left(\rho_n^2+\rho_p^2\right)\right] \right.$$

$$+ \frac{1}{12}t_3\rho^\alpha\left[\left(1+\frac{1}{2}x_3\right)\rho^2 - \left(x_3+\frac{1}{2}\right)\right]\left(\rho_n^2+\rho_p^2\right) + \frac{1}{4}\left[t_1\left(1+\frac{1}{2}x_1\right) + t_2\left(1+\frac{1}{2}x_2\right)\right]\tau_p$$

$$+ \frac{1}{4}\left[t_2\left(x_2+\frac{1}{2}\right) - t_1\left(x_1+\frac{1}{2}\right)\right]\left(\tau_n\rho_n + \tau_p\rho_p\right) \frac{1}{16}\left[3t_1\left(1+\frac{1}{2}x_1\right) - t_2\left(1+\frac{1}{2}x_2\right)\right](\nabla\rho)^2$$

$$- \frac{1}{16}\left[3t_1\left(x_1+\frac{1}{2}\right) + t_2\left(x_2+\frac{1}{2}\right)\right]\left[(\nabla\rho_n)^2 + (\nabla\rho_p)^2\right]$$

$$\left. + \frac{1}{2}W_0\left[J\cdot\nabla\rho + J_n\cdot\nabla\rho_n + J_p\cdot\nabla\rho_p\right]\right\}, \qquad (11)$$

with

$$\begin{aligned} \tau &= \tau_n + \tau_p && \textit{kinetic energy densities} \\ \rho &= \rho_n + \rho_p && \textit{local nucleon densities.} \\ J &= J_n + J_p && \textit{spin-orbit densities} \end{aligned} \qquad (12)$$

Coulomb part depends only on the charge density and assigned as a sum of the direct term and exchange term. The contribution of the exchange term is since the Coulomb interaction is an infinite range. The Coulomb energy is given by [27]

$$\varepsilon_{Coul} = \varepsilon_{Coul}^{dir} + \varepsilon_{Coul}^{ex}. \qquad (13)$$

The direct and exchange terms are given by

$$\varepsilon_{Coul}^{dir} = \frac{e^2}{2}\iint \frac{\rho_p(r)\rho_p(r')}{|r-r'|}dr\,dr', \qquad (14)$$

$$\varepsilon_{Coul}^{ex} = -\frac{4}{3}e^2\left(\frac{3}{\pi}\right)^{1/3}\int \rho_p(r)^{4/3}dr, \qquad (15)$$

where $e^2 = 1.44$ MeV·fm.

The center of mass-energy is given by [28]

$$\varepsilon_{cm} = \frac{\langle P_{cm}^2\rangle}{2Am}, \qquad (16)$$

with

$$\langle P_{cm}^2\rangle = \sum w_\beta \langle\varphi_\beta|P^2|\varphi_\beta\rangle - \sum\left(w_\alpha w_\beta + \sqrt{w_\alpha(1-w_\alpha)\,w_\beta(1-w_\beta)}\right)\left|\langle\varphi_\alpha|P^2|\varphi_\beta\rangle\right|^2, \qquad (17)$$

where $P_{cm} = \sum_i P_i$ is the total momentum operator of the center of mass, P is the momentum operator, m is the average nucleon mass, A is the nucleon number, w_α and w_β are the occupation probabilities of the states φ_α and φ_β, respectively.

Pairing is a key ingredient in a mean-field description of nuclear structure [29]. It is especially important in the case of partially open shells with a high density of almost degenerated states. There are two widely used methods to treat pairing. The first one is the HFB method [8], where pairing correlations are included by introducing the concept of independent quasiparticles defined by the Bogolyubov transformation. The second one is the BCS approximation, which is a simplification of HFB for time-reversal-invariant systems [9]. The effective pairing interaction is given by a two-body zero-range local force including a density dependence as [30]:

$$V_{pair,q}(r_1,r_2) = \frac{V_0}{2}\left[1 - V_1\left(\frac{\rho(r)}{\rho_{0,pair}}\right)^\gamma\right]\delta(r_1-r_2). \qquad (18)$$

The pairing energy of the two-nucleon interaction is given by [15, 25]:

$$\varepsilon_{Pair} = \sum_{q\in\{p,n\}} \frac{V_{pair,q}(r_1,r_2)}{4}\int d^3r\,\chi_q^2(r)F(r), \qquad (19)$$

where

$$\chi_q^2 = \sum_{\alpha \in q} f_\alpha u_\alpha v_\alpha |\varphi_\alpha|^2 , \quad (20)$$

$$F(r) = \begin{cases} 1 & \text{for volume pairing} \\ 1 - \rho(r)/\rho_c & \text{for surface pairing} \end{cases} . \quad (21)$$

The strength $V_{pair,q}$ is adjusted for each Skyrme parameterization. The term $\rho_{0,pair}$ represents the nuclear saturation density that is typically equal to $\rho_c = 0.16\ \text{fm}^{-3}$, while $\chi(r)$ and $\rho(r)$ are the pairing and particle densities, respectively. φ_α is the single-particle state, f_α is the phase-space weight, v_α and u_α are the occupation and non-occupation amplitudes, respectively; with $u_\alpha^2 + v_\alpha^2 = 1$.

The charge, neutron and proton densities in spherical representation are given by [24]

$$\rho_k(r) = \sum_{\beta \in k} w_\beta \varphi_\beta(r)^* \varphi_\beta(r) \ , \ k = n \text{ or } p, \quad (22)$$

where k denote to the neutrons or protons of the nucleus. The total CDD is given by [31, 32]

$$\rho_{ch}(r) = \rho_{ch}^p(r) + \rho_{ch}^n(r), \quad (23)$$

and the proton and neutron parts of the total CDD have the forms

$$\rho_{ch}^p(r) = \int \rho_{point,p}(r - r') \rho_p(r') dr', \quad (24)$$

$$\rho_{ch}^n(r) = \int \rho_{point,n}(r - r') \rho_n(r') dr', \quad (25)$$

where $\rho_{point,p}(r - r')$ and $\rho_{point,n}(r - r')$ are the point-like proton and neutron densities, respectively; while $\rho_p(r')$ and $\rho_n(r')$ are the proton and neutron density distributions, respectively.

The charge form factors are obtained in terms of the ground-state CDDs, where the form factor is simply transformed to the CDD with using the Fourier - Bessel transformations and vice versa [6]. Therefore:

$$F_{ch}(q) = \frac{4\pi}{Z} \int_0^\infty \rho_{ch}\, j_0(qr) r^2 dr , \quad (26)$$

where $j_0(qr) = \sin(qr)/qr$ is the zeroth-order spherical Bessel function and q is the momentum transfer from the incident electron to the target nucleus. In the limit $q \to 0$, the target will be represented as a point particle, and the form factor of this target is equal to unity $F(q \to 0) = 1$.

3. Results and discussion

In the present work, several nuclear ground-state properties of $^{24-42}$Si isotopes have been studied using SHF and HFB methods. Firstly, we have calculated the charge, proton, neutron, and mass density distributions in addition to the corresponding radii using the SHF method. Moreover, the binding energy per nucleon, the neutron skin thickness, and the charge form factors are calculated with the same method. These calculations are performed by using nine types of Skyrme parameterizations listed in Table 1. The charge density distributions are calculated for ^{28}Si and ^{30}Si nuclei and plotted in Fig. 1, where the available experimental data for these nuclei are obtained using the Fourier - Bessel model-independent analysis [33]. The experimental data are very well interpreted by the calculations with SkM* that denoted by the black curves with neglecting the slight depression at the small regions of *r*, where the data are located higher than the calculations. The central depressions appearing in density distributions are associated with the occupations of s-orbits [34]. The inset figures are implied to show independently the agreement between the calculations with SkM* and the data. According to the deduced results of the CDD of ^{28}Si and ^{30}Si nuclei, and as a result of the lack of experimental data for the other Si-isotopes, it is preferable to apply the SkM* parameterization to calculate the charge, proton, neutron and mass density distributions of all other isotopes.

Table 1. **The Skyrme parameterizations that have been used in this work**

Parameter	t_0, MeV·fm^3	t_1, MeV·fm^5	t_2, MeV·fm^5	t_3, MeV·fm$^{3\alpha}$	W_0, MeV·fm^5	χ_0	χ_1	χ_2	χ_3	α
SkB [35]	–1602.780	570.880	–67.700	8000.0	125.0	–0.165	0.0	0.0	–0.286	0.333
SkM* [9]	–2645.0	410.0	–135.0	15595.0	130.0	0.09	0.0	0.0	0.0	0.167
SkE [36]	–1140.250	309.610	–122.220	11608.100	111.450	0.798	0.0	0.0	1.632	0.800
SkX [37]	–1445.322	246.867	–131.786	12103.863	148.637	0.340	0.580	0.127	0.030	0.500
SLy4 [38]	–2488.910	486.820	–546.390	13777.000	123.000	0.834	–0.344	–1.000	1.354	0.167
Skxta [39]	–1443.180	257.229	–137.843	12139.420	180.441	0.341	0.580	0.167	0.0	0.500
SkP [40]	–2931.700	320.620	–337.410	18708.970	100.000	0.292	0.653	–0.537	0.181	0.167
UNEDF0 [41]	–1883.688	277.500	608.431	13901.948	33.9006	0.00974	–1.778	–1.677	–0.381	0.322
UNEDF1 [42]	–2078.328	239.401	1575.120	14263.646	109.685	0.0538	–5.077	–1.367	–0.163	0.270

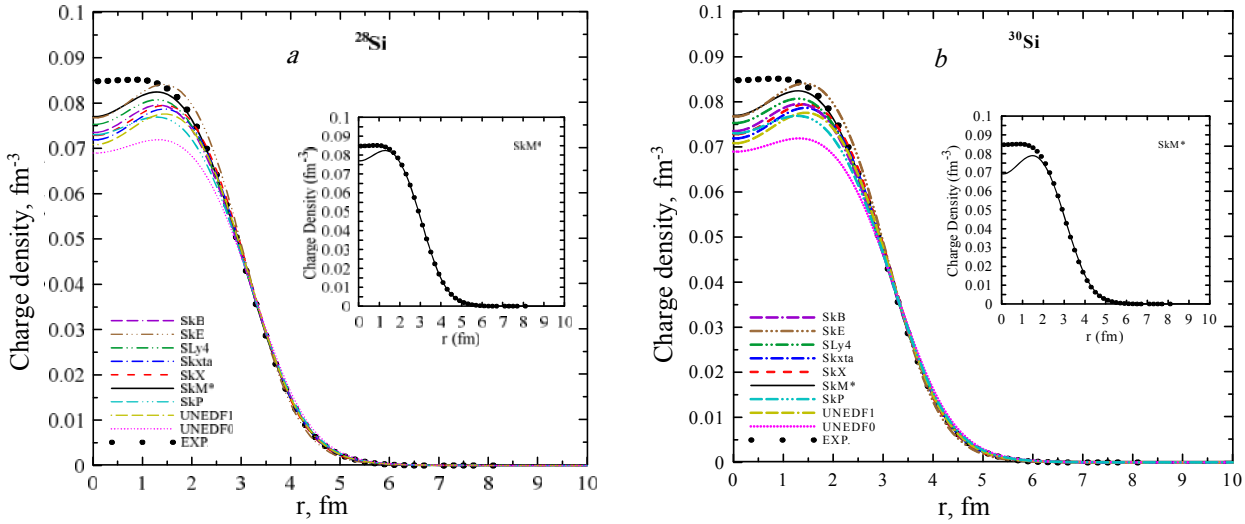

Fig. 1. Charge density distributions for ^{28}Si (*a*) and ^{30}Si (*b*). The inset figures are plotted to show the agreement between the calculations with SkM* and experimental data. The experimental data are taken from Ref. [33]. (See color Figure on the journal website.)

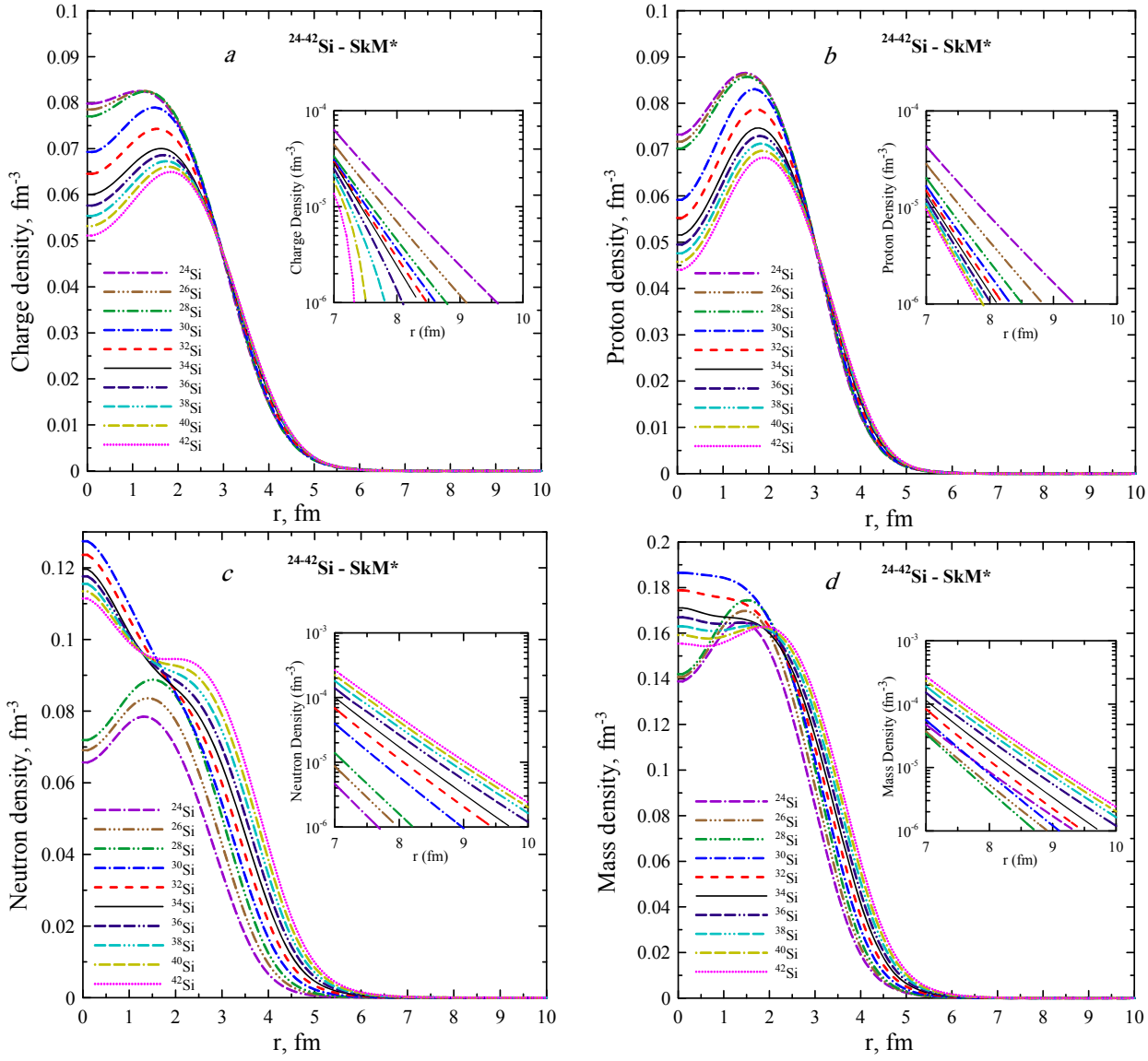

Fig. 2. Calculated density distributions for $^{24-42}$Si isotopes. The inset is in logarithmic scale: *a* – charge densities; *b* – proton densities; *c* – neutron densities; *d* – mass densities. (See color Figure on the journal website.)

Fig. 2 shows the calculated density profiles that are classified as the charge, proton, neutron, and mass density distributions, respectively. All density curves are obtained using SkM* parameterization. The inset figures have been embedded to show large scales of the overlapped curves at the tail regions ($r \geq 7$ fm) of the density distributions. The effects of increasing the neutron number on the charge and proton density distributions are explained by the Fig. 2 (*a* and *b*), respectively; where these distributions are decreased gradually for the sequence isotopes especially at the central and tail regions. The density distributions of neutrons and nuclear mass are presented in Fig. 2 (*c* and *d*), respectively. Adding neutrons to ^{24}Si nucleus up to more neutron-rich ^{42}Si isotope extending the densities exclusively at the fall-off and the surface regions. At the central regions of the neutron and mass density distributions there are distinctive gaps between $^{24-28}$Si curves and these of $^{30-42}$Si, as well as the densities of ^{24}Si - ^{28}Si, increasing and these of ^{30}Si - ^{42}Si decreasing successively as neutron number increasing. These discrepancies may be attributed to the redistributions of the nucleons as a result of the nuclear interaction with the additional neutrons and to the increasing of the quadrupole deformation of these isotopes, especially beyond the stable ^{28}Si isotope. The proton and neutron density distributions for the stable Z = N ^{28}Si nucleus are very similar along with all *r* values. The charge density and proton density curves for all investigated isotopes, and the neutron density and mass density curves for $^{24-28}$Si isotopes, are increasing progressively from $r = 0$ fm to form humps at the central regions of the nuclei around $r \approx 1.5$ fm and then these curves are sloped steeply beyond this point. The neutron density and mass density curves for $^{30-42}$Si isotopes exhibited a steep slope behavior along with all values of *r*.

The calculated rms charge radii and binding energy per nucleon (BE/A) are given in Table 2 together with the available experimental values. The smallest charges radii and the biggest BE/A are associated with the nuclei that are stable or located near the stability line in the nuclear chart of isotopes. The calculated values using SkM* are very close to the experimental ones in comparison with the other calculated results.

Table 2. **Calculated rms charge radii and binding energy per nucleon**

A			24	26	28	30	32	34	36	38	40	42
rms charge radii, fm	Calc.	SkB	3.174	3.160	3.151	3.184	3.213	3.242	3.248	3.255	3.261	3.267
		SkM*	3.156	3.128	3.129	3.135	3.176	3.217	3.225	3.233	3.242	3.251
		SkE	3.044	3.037	3.041	3.076	3.114	3.153	3.165	3.165	3.191	3.203
		SkX	3.147	3.117	3.104	3.123	3.163	3.204	3.213	3.225	3.237	3.250
		Sly4	3.181	3.152	3.136	3.151	3.189	3.226	3.236	3.246	3.256	3.265
		Skxta	3.169	3.140	3.111	3.144	3.176	3.213	3.223	3.235	3.249	3.264
		SkP	3.235	3.200	3.183	3.205	3.252	3.260	3.275	3.287	3.298	3.309
		UNEDF0	3.316	3.264	3.240	3.241	3.274	3.282	3.299	3.326	3.342	3.360
		UNEDF1	3.233	3.171	3.143	3.220	3.211	3.231	3.243	3.257	3.268	3.315
	EXP. [43]				3.1224 ± 0.0024	3.1336 ± 0.004						
BE/A, MeV	Calc.	SkB	7.149	7.665	8.182	8.393	8.410	8.489	8.268	8.115	8.019	7.970
		SkM*	7.179	7.928	8.461	8.553	8.478	8.315	8.110	7.864	7.641	7.382
		SkE	7.291	7.899	8.465	8.655	8.538	8.460	8.212	8.005	7.833	7.689
		SkX	7.007	7.695	8.234	8.615	8.504	8.410	8.074	7.683	7.626	7.435
		Sly4	7.144	7.794	8.335	8.426	8.395	8.362	8.129	7.818	7.588	7.458
		Skxta	7.018	7.736	8.291	8.471	8.394	8.442	8.057	7.823	7.611	7.415
		SkP	6.865	7.491	7.992	5.762	6.275	8.187	7.901	7.651	7.430	7.235
		UNEDF0	6.293	6.844	7.275	7.542	7.633	7.835	7.487	7.060	6.788	6.546
		UNEDF1	6.820	7.480	7.982	7.650	8.092	8.221	7.898	7.593	7.420	6.811
	EXP. [44]		7.167	7.925	8.448	8.521	8.482	8.336	8.114	7.890	7.661	7.372

Fig. 3 provides us a clear perception of the effect of increasing the neutron number on the differences between the rms neutron radii and rms proton radii. These differences represent the neutron skin thicknesses that are referred to as the surplus of neutrons at the surface regions of nuclei. Fig. 3 shows the almost linear dependence of the variation of neutron skin thickness as increasing the mass number A of the nuclei which includes the neutron number. The negative values for ^{24}Si, ^{26}Si, and ^{28}Si nuclei indicate that the proton rms radii are larger than the neutron rms radii.

The form factors are considered as a strong test for the applicability of the nuclear models and provide significant maps of the nuclear structure. The inner structure of the nuclei can be identified in terms of the elastic charge form factors obtained by the Fourier transform of the spatial charge density distributions [6]. The theoretical calculations of the charge form factors, which performed in terms of SkM* parameterization, are plotted in Fig. 4. All curves beyond that of the ^{24}Si nucleus are progressively offset by 10^2 in the form factor to show the calculated results

explicitly. As a result of increasing the neutron number from ^{24}Si to ^{42}Si isotopes, the diffraction minima and maxima values of all curves are shifted to low values of momentum transfer q. These effects are noticed in the central regions of the CDD that presented in Fig. 2, *a*, where the humps of the consecutive curves are increased progressively up to that of the ^{42}Si isotope. So, the charge form factors are very sensitive to the effects of changing the neutron number as the sensitivity of the CDD to the same effects. The available experimental data for ^{28}Si and ^{30}Si nuclei are presented in Fig. 4. The data of ^{30}Si are explained excellently by the calculations for all q regions and the calculations agree very well with the data of ^{28}Si for the most regions of q except the slight deviation that appears beyond $q \approx 2.8$ fm^{-1}.

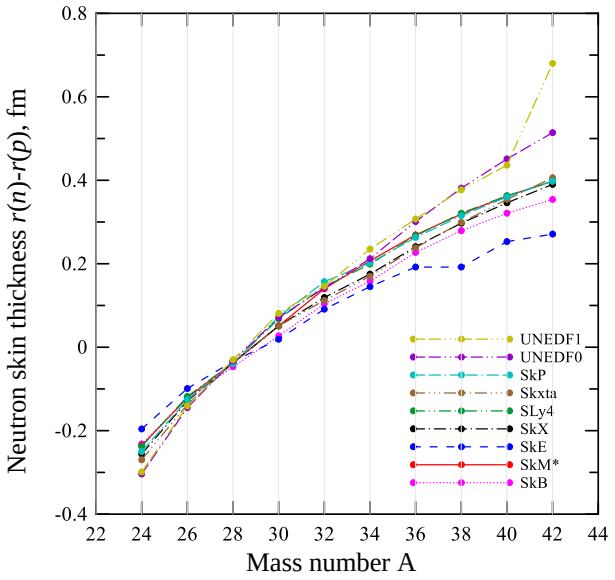

Fig. 3. Calculated neutron skin thickness $r(n)$-$r(p)$ for $^{24\text{-}42}$Si isotopes. (See color Figure on the journal website.)

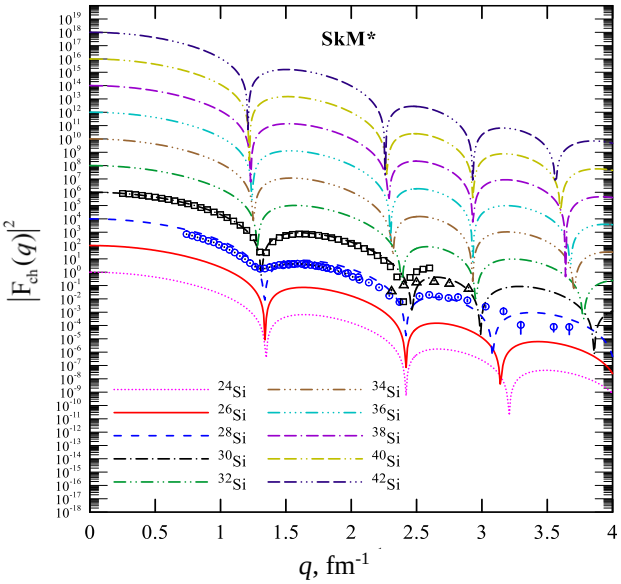

Fig. 4. Calculated charge form factors for ^{24}Si, ^{26}Si ($\times 10^2$), ^{28}Si ($\times 10^4$), ^{30}Si ($\times 10^6$), ^{32}Si ($\times 10^8$), ^{34}Si ($\times 10^{10}$), ^{36}Si ($\times 10^{12}$), ^{38}Si ($\times 10^{14}$), ^{40}Si ($\times 10^{16}$), and ^{42}Si ($\times 10^{18}$). The circles are the experimental data of ^{28}Si that are taken from Ref. [45]. The squares and triangles are the experimental data of ^{30}Si that are taken from Ref. [33] and Ref. [46], respectively. (See color Figure on the journal website.)

The HFB method with Skyrme forces is used to study the shape of the selected Si-isotopes. The potential energy curves (PECs) as a function of the quadrupole deformation parameter β_2 are calculated using the HFB method with SkM* Skyrme force. The calculations are performed using HFBTHO code [12] that deals with the axially deformed configurational HFB calculations, where the HFB wave functions are expanded in a complete set of transformed harmonic oscillator (THO) states [10]. The quadrupole deformation parameter β_2 is widely used to describe the deformation of the nuclei than the mass quadrupole moments Q and the relation between these quantities is given by [25]

$$\beta_2 = \sqrt{\frac{\pi}{5}} \frac{Q}{A\langle r^2 \rangle}, \qquad (27)$$

where $\langle r^2 \rangle$ is the nucleus mean square radius.

The obtained PECs for $^{24\text{-}42}$Si isotopes are displayed in Fig. 5, where β_2 is ranging between –0.4 and 0.4. The PEC for ^{24}Si has two minima on the oblate and prolate sides at $\beta_2 = -0.15$ and $\beta_2 = 0.15$, respectively, with a small hump in the middle at $\beta_2 = 0$. The energy variation between these regions β_2 is about 0.036 MeV. So, the nucleus ^{24}Si has oblate-prolate shape coexistence. Oblate shapes are found in ^{26}Si and ^{28}Si, where the oblate deformation minima of the PECs correspond to β_2 values equal to –0.2 and –0.25, respectively. The oblate deformation grows as increasing the neutron number for ^{26}Si - ^{28}Si. The uniform and symmetric curve of ^{30}Si in the spherical minimum region indicates that this nucleus is very close to spherical shape. The spherical minima found in ^{32}Si and ^{34}Si around $\beta_2 = 0$ indicate that these nuclei have spherical shapes, where ^{34}Si has a shell closure at neutron magic number $N = 20$. Furthermore, the PEC shape for ^{36}Si reveals that this nucleus has a spherical shape even though the small flat region confined between $\beta_2 = -0.1$ and $\beta_2 = 0.1$. The PECs curves for ^{38}Si and ^{40}Si have two minima forming a coexistence of prolate and oblate deformations

located at $\beta_2 = -0.14$ and $\beta_2 = 0.2$ for ^{38}Si and $\beta_2 = -0.2$ and $\beta_2 = 0.2$ for ^{40}Si. These two minima are separated by excitation energies of 0.188 and 0.252 MeV for ^{38}Si and ^{40}Si, respectively. The last figure related to ^{42}Si nucleus and this figure exhibits an explicit oblate deformation represented by the oblate minimum located at $\beta_2 = 0.24$. Although ^{42}Si nucleus has a shell closure at neutron magic number $N = 28$, this nucleus is deformed because of its proximity to the neutron drip-line region, where the nuclei in this region of the nuclear landscape become more deformed and unstable to neutron decay.

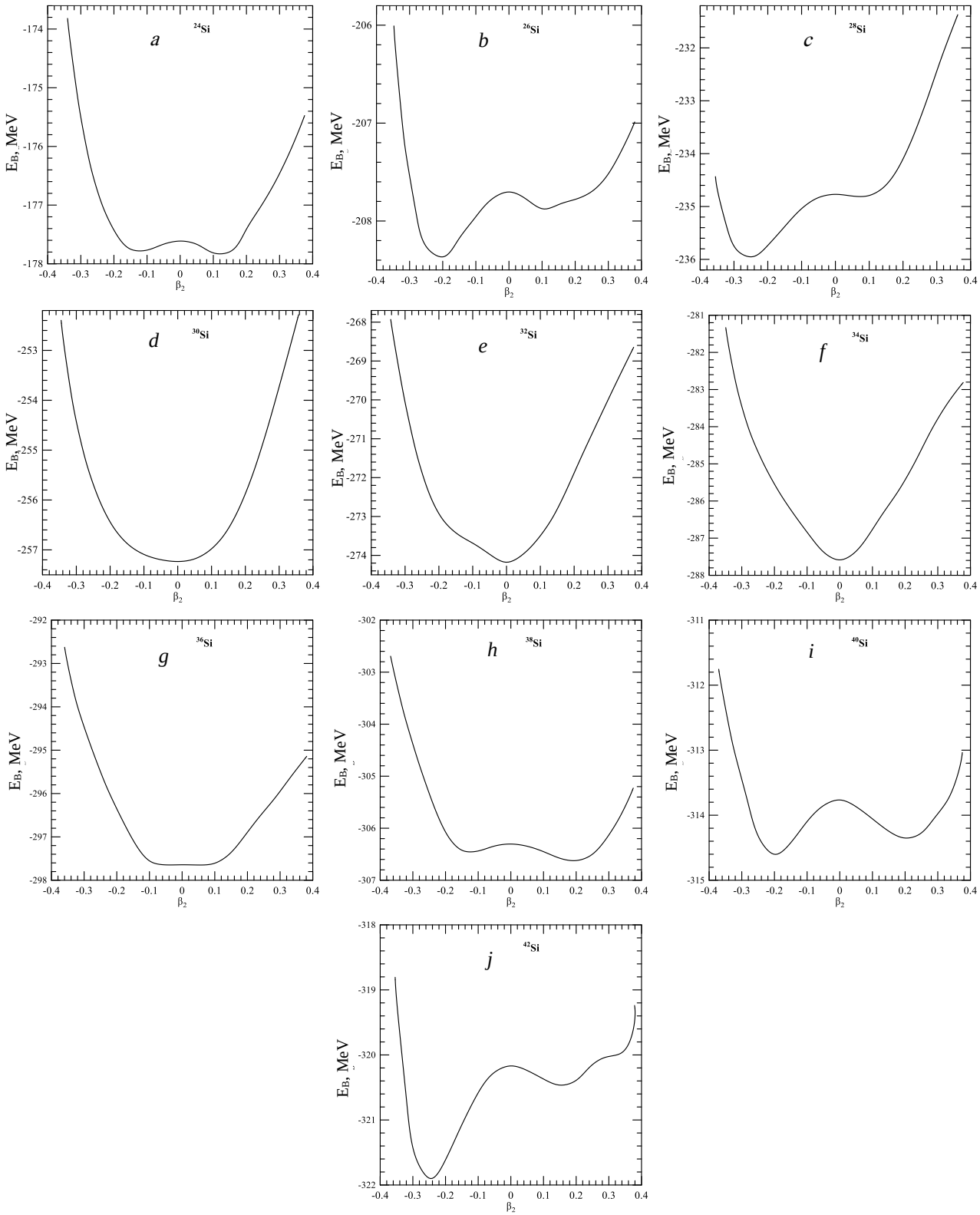

Fig. 5. Calculated potential energy curves for $^{24\text{-}42}$Si isotopes using SkM* parameterization.

4. Conclusions

The ground-state properties have been studied for some even-even Si-isotopes using the SHF method. The HFB method has been used to study the shape of nuclei in terms of the PECs that plotted as a function of the quadrupole deformation parameters. All studied properties are very important in gathering comprehensive concepts about the nuclear structure of the selected isotopes. The calculated CDD and charge form factors with SkM* Skyrme force for ^{28}Si and ^{30}Si nuclei are in very good agreement with the experimental data. The CDD is decreased gradually for the sequence isotopes at the central and tail regions as increased the neutron number. The obtained results of the rms charge radii and binding energy per nucleon are very close to the experimental ones. Our calculations confirmed that the stable isotopes have the smallest values of charge radii and the biggest values of binding energies. The calculations revealed the linear dependence of the neutron skin thickness as a function of the variation of neutron number. The obtained PECs showed that the ^{30}Si, ^{32}Si and ^{34}Si isotopes have spherical shapes confirmed by the spherical minima around $\beta_2 = 0$. ^{36}Si nucleus has also a shape closer to the spherical shape. Our calculations showed that the ^{26}Si, ^{28}Si and ^{42}Si isotopes have oblate deformations while the ^{24}Si, ^{38}Si and ^{40}Si isotopes have oblate-prolate shape coexistence.

The authors would like to express their deepest gratitude to the Directorate of Nuclear Researches and Applications, Ministry of Science and Technology, for supporting this work.

REFERENCES

1. P. Ring, P. Schuck. *The Nuclear Many-Body Problem* (Springer Science & Business Media, 2004) 716 p.
2. J.-P. Blaizot, G. Ripka. *Quantum Theory of Finite Systems* (MIT press Cambridge, MA, 1986) 657 p.
3. T.H.R. Skyrme. The effective nuclear potential. Nucl. Phys. 9 (1958) 615.
4. D. Vautherin, D.M. Brink. Hartree-Fock calculations with Skyrme's interaction. I. Spherical nuclei. Phys. Rev. C 5 (1972) 626.
5. C.B. Dover, N. Van Giai. The nucleon-nucleus potential in the Hartree-Fock approximation with Skyrme's interaction. Nucl. Phys. A 190 (1972) 373.
6. T. Deforest Jr, J.D. Walecka. Electron scattering and nuclear structure. Adv. Phys. 15(57) (1966) 1.
7. K.W. Schmid, P.G. Reinhart. Center-of-mass projection of Skyrme-Hartree-Fock densities. Nucl. Phys. A 530 (1991) 283.
8. A.L. Goodman. Hartree-Fock-Bogoliubov Theory with Applications to Nuclei. Advances in Nuclear Physics 11 (1979) 263.
9. J. Bartel et al. Towards a better parametrisation of Skyrme-like effective forces: A critical study of the SkM force. Nucl. Phys. A 386 (1982) 79.
10. M.V. Stoitsov, W. Nazarewicz, S. Pittel. New discrete basis for nuclear structure studies. Phys. Rev. C 58 (1998) 2092.
11. M.V. Stoitsov et al. Quadrupole deformations of neutron-drip-line nuclei studied within the Skyrme Hartree-Fock-Bogoliubov approach. Phys. Rev. C 61 (2000) 034311.
12. M.V. Stoitsova et al. Axially deformed solution of the Skyrme-Hartree-Fock-Bogolyubov equations using the transformed harmonic oscillator basis. The program HFBTHO (v1. 66p). Comput. Phys. Commun. 167 (2005) 43.
13. Y. Yulianto, Z. Su'ud. Nuclear binding energy and density distribution of Pb isotopes in a Skyrme-Hartree-Fock method. Nucl. Phys. At. Energy 18 (2017) 151.
14. Y. Yulianto, Z. Su'ud. Radii and Density Calculations of ^{209}Bi by Using Skyrme-Hartree-Fock Method. J. Phys. Conf. Ser. 799 (2017) 12024.
15. A.N. Abdullah. Matter density distributions and elastic form factors of some two-neutron halo nuclei. Pramana 89 (3) (2017) 43.
16. A.H. Taqi, E.G. Khidher. Ground and transition properties of ^{40}Ca and ^{48}Ca nuclei. Nucl. Phys. At. Energy 19 (2018) 326.
17. A.A. Alzubadi, R.A. Radhi, N.S. Manie. Shell model and Hartree-Fock calculations of longitudinal and transverse electroexcitation of positive and negative parity states in ^{17}O. Phys. Rev. C 97 (2018) 024316.
18. T. Bayram, A.H. Yilmaz. Shape of Te isotopes in mean-field formalism. Pramana 83(6) (2014) 975.
19. Y. El Bassem, M. Oulne. Ground-state properties of even-even and odd Nd, Ce, and Sm isotopes in Hartree-Fock-Bogoliubov method. Int. J. Mod. Phys. E 24(10) (2015) 1550073.
20. Y. El Bassem, M. Oulne. Hartree-Fock-Bogoliubov calculation of ground-state properties of even-even and odd Mo and Ru isotopes. Nucl. Phys. A 957 (2017) 22.
21. M. Ouhachi et al. Nuclear structure investigation of neutron-rich Mn isotopes. Chinese J. Phys. 56 (2018) 574.
22. W. Greiner, J.A. Maruhn. *Nuclear Models* (Springer, 1996).
23. H. Aytekin, R. Baldik, H. Alici. On the nuclear properties of ^{32}S, ^{64}Zn, ^{67}Zn, ^{89}Y, ^{90}Zr and ^{153}Eu targets used for production of ^{32}P, ^{64}Cu, ^{67}Cu, ^{89}Sr, ^{90}Y, and ^{153}Sm therapeutic radionuclides. Ann. Nucl. Energy 46 (2012) 128.
24. P.-G. Reinhard et al. Shape coexistence and the effective nucleon-nucleon interaction. Phys. Rev. C 60 (1999) 014316.

25. J. Erler, P. Klupfel, P.G. Reinhard. Self-consistent nuclear mean-field models: example Skyrme-Hartree-Fock. J. Phys. G 38 (2011) 33101.
26. M. Brack, C. Guet, H.B. Hakansson. Selfconsistent semiclassical description of average nuclear bulk properties – a link between microscopic and macroscopic models. Phys. Rep. 123 (1985) 275.
27. E.B. Suckling. Nuclear Structure and Dynamics from the Fully Unrestricted Skyrme-Hartree-Fock Model (Ph.D. Thesis, Univ. of Surrey, 2011).
28. M. Beiner et al. Nuclear ground-state properties and self-consistent calculations with the Skyrme interaction: (I). Spherical description. Nucl. Phys. A 238 (1975) 29.
29. A. Bohr, B.R. Mottelson, D. Pines. Possible analogy between the excitation spectra of nuclei and those of the superconducting metallic state. Phys. Rev. 110 (1958) 936.
30. A.A. Alzubadi, A.A. Abdulhasan. Nuclear deformation study using the framework of self-consistence Hartree-Fock-Bogoliubov. Karbala Int. J. Mod. Sci. 1 (2015) 110.
31. L.R.B. Elton. *Nuclear Size* (London: Oxford University Press, 1961)114 p.
32. A.N. Antonov. Charge density distributions and related form factors in neutron-rich light exotic nuclei. Int. J. Mod. Phys. E 13 (2004) 759.
33. H. De Vries, C.W. De Jager, C. De Vries. Nuclear charge-density-distribution parameters from elastic electron scattering. At. Data. Nucl. Data Tables 36 (1987) 495.
34. B. Schuetrumpf, W. Nazarewicz, P.-G. Reinhard. Central depression in nucleonic densities: Trend analysis in nuclear density-functional-theory approach. Phys. Rev. C 96 (2017) 024306.
35. H.S. Kohler. Skyrme force and the mass formula. Nucl. Phys. A 258 (1976) 301.
36. J. Friedrich, P.-G. Reinhard. Skyrme-force parametrization: Least-squares fit to nuclear ground-state properties. Phys. Rev. C 33 (1986) 335.
37. B.A. Brown. New Skyrme interaction for normal and exotic nuclei. Phys. Rev. C 58 (1998) 220.
38. E. Chabanat. A Skyrme parametrization from subnuclear to neutron star densities Part II. Nuclei far from stabilities. Nucl. Phys. A 635 (1998) 231.
39. B.A. Brown et al. Tensor interaction contributions to single-particle energies. Phys. Rev. C 74 (2006) 061303.
40. J. Dobaczewski, H. Flocard, J. Treiner. Hartree-Fock-Bogolyubov description of nuclei near the neutron-drip line. Nucl. Phys. A 422 (1984) 103.
41. M. Kortelainen et al. Nuclear energy density optimization. Phys. Rev. C 82 (2010) 024313.
42. M. Kortelainen et al. Nuclear energy density optimization: Large deformations. Phys. Rev. C 85 (2012) 024304.
43. I. Angeli, K.P. Marinova. Table of experimental nuclear ground-state charge radii: An update. At. Data. Nucl. Data Tables 99 (2013) 69.
44. M. Wang et al. The Ame2012 atomic mass evaluation. Chinese Phys. C 36 (2012) 1603.
45. G.C. Li, M.R. Yearian, I. Sick. High-momentum-transfer electron scattering from ^{24}Mg, ^{27}Al, ^{28}Si, and ^{32}S. Phys. Rev. C 9 (1974) 1861.
46. J. Wesselling et al. 2s1/2 occupancies in ^{30}Si, ^{31}P, and ^{32}S. Phys. Rev. C 55 (1997) 2773.

Алі А. Абдул Хасан[1], Ехсан М. Рахім[1,*], Саад С. Давуд[1], Акіл М. Джарі[1], Раша З. Ахмед[2]

[1] Міністерство науки і технологій, Управління ядерних досліджень і програм, Багдад, Ірак
[2] Університет Багдаду, Коледж освіти для жінок,
кафедра управління людськими ресурсами, Багдад, Ірак

*Відповідальний автор: ehsan.nucl@yahoo.com

ДОСЛІДЖЕННЯ ЯДЕРНОЇ СТРУКТУРИ ПАРНО-ПАРНИХ ІЗОТОПІВ $^{24-42}$Si З ВИКОРИСТАННЯМ МЕТОДІВ СКІРМА - ХАРТРІ – ФОКА ТА ХАРТРІ - ФОКА - БОГОЛЮБОВА

Досліджено властивості основних станів ядер та ядерні деформації деяких парно-парних ізотопів кремнію. Сферичний метод Скірма - Хартрі - Фока, що включає обчислення Хартрі - Фока на додаток до декількох загальних параметризацій Скірма, таких як SkB, SkM*, SkE, SkX, SLy4, Skxta, SkP, UNEDF0 і UNEDF1, був використаний для обчислення розподілу густини заряду основних ядерних станів та пов'язаних зарядових радіусів для ^{28}Si і ^{30}Si завдяки наявності експериментальних даних для цих двох стабільних ізотопів. Крім того, масові, нейтронні та протонні густини з пов'язаними з ними радіусами, енергіями зв'язку, поверхневими нейтронними товщинами та зарядовими форм-факторами було розраховано для ізотопів $^{24-42}$Si з використанням параметризації SkM*. Досліджено квадрупольні деформації вибраних ізотопів у термінах кривих потенційної енергії, виведені як функції параметрів квадрупольної деформації за допомогою обчислень Хартрі - Фока - Боголюбова в аксіально деформованій конфігурації з параметром SkM*.

Ключові слова: властивості основного стану ядра, Скірма - Хартрі - Фок, Хартрі - Фок - Боголюбов, квадрупольна деформація, ізотопи кремнію.

Али А. Абдул Хасан[1], Эхсан М. Рахим[1,*], Саад С. Давуд[1], Акил М. Джари[1], Раша З. Ахмед[2]

[1] Министерство науки и технологий, Управление ядерных исследований и программ, Багдад, Ирак
[2] Университет Багдада, Колледж образования для женщин,
кафедра управления человеческими ресурсами,
Багдад, Ирак

*Ответственный автор: ehsan.nucl@yahoo.com

ИССЛЕДОВАНИЯ ЯДЕРНОЙ СТРУКТУРЫ ЧЕТНО-ЧЕТНЫХ ИЗОТОПОВ $^{24-42}$Si С ИСПОЛЬЗОВАНИЕМ МЕТОДОВ СКИРМА - ХАРТРИ – ФОКА И ХАРТРИ - ФОКА - БОГОЛЮБОВА

Исследованы свойства основных состояний ядер и ядерные деформации некоторых парно-четных изотопов кремния. Сферический метод Скирма - Хартри - Фока, включающий вычисления Хартри - Фока в дополнение к нескольким общим параметризациям Скирма, таких как SkB, SkM* SkE, SkX, SLy4, Skxta, SkP, UNEDF0 и UNEDF1, был использован для вычисления распределения плотности заряда основных ядерных состояний и связанных зарядовых радиусов для ^{28}Si и ^{30}Si благодаря наличию экспериментальных данных для этих двух стабильных изотопов. Кроме того, массовые, нейтронные и протонные плотности со связанными с ними радиусами, энергиями связи, поверхностными нейтронными толщинами и зарядовыми форм-факторами были рассчитаны для изотопов $^{24-42}$Si с использованием параметризации SkM*. Исследованы квадрупольные деформации выбранных изотопов в терминах кривых потенциальной энергии, выведены как функции параметров квадрупольной деформации с помощью вычислений Хартри - Фока - Боголюбова в аксиально деформированной конфигурации с параметром SkM*.

Ключевые слова: свойства основного состояния ядра, Скирма - Хартри - Фок, Хартри - Фок - Боголюбов, квадрупольная деформация, изотопы кремния.

Надійшла / Received 25.07.2019